nature nanotechnology

ARTICLES

PUBLISHED ONLINE: 30 SEPTEMBER 2012 | DOI: 10.1038/NNANO.2012.161

# Low-resistance spin injection into silicon using graphene tunnel barriers

O. M. J. van 't Erve*, A. L. Friedman†, E. Cobas†, C. H. Li, J. T. Robinson and B. T. Jonker*

**Spin manipulation in a semiconductor offers a new paradigm for device operation beyond Moore's law. Ferromagnetic metals are ideal contacts for spin injection and detection, but the intervening tunnel barrier required to accommodate the large difference in conductivity introduces defects, trapped charge and material interdiffusion, which severely compromise performance. Here, we show that single-layer graphene successfully circumvents the classic issue of conductivity mismatch between a metal and a semiconductor for electrical spin injection and detection, providing a highly uniform, chemically inert and thermally robust tunnel barrier. We demonstrate electrical generation and detection of spin accumulation in silicon above room temperature, and show that the contact resistance–area products are two to three orders of magnitude lower than those achieved with oxide tunnel barriers on silicon substrates with identical doping levels. Our results identify a new route to low resistance–area product spin-polarized contacts, a key requirement for semiconductor spintronic devices that rely on two-terminal magnetoresistance, including spin-based transistors, logic and memory.**

The spin angular momentum of an electron has been identified as a potential new state variable in semiconductor device operation for use beyond Moore's law[1–3], and new paradigms for spin-based device operation have been proposed and modelled[4–8]. Ferromagnetic metals, which exhibit intrinsically spin-polarized electron populations, high Curie temperatures and low coercive fields, are seemingly ideal candidates as contacts for electrical injection and detection of spin currents in the semiconductor channel. However, the large difference in conductivity between metal and semiconductor makes this impossible[9–11].

A tunnel barrier between the ferromagnetic metal and the semiconductor has been identified as a potential solution to this problem[9–11], and extensive effort has therefore been directed towards developing appropriate tunnel barriers for spin contacts. Most work has focused on a reverse-biased ferromagnetic Schottky barrier[12,13] or an insulating oxide layer such as $Al_2O_3$ or MgO with a ferromagnetic metal contact[14–17]. For example, we have recently shown that $SiO_2$, an oxide widely used in the electronics industry, serves as an excellent spin tunnel barrier in ferromagnetic metal/$SiO_2$/Si structures[18], although the oxide thickness required to achieve a good spin signal resulted in high contact resistance–area products.

An ideal tunnel barrier should exhibit the following key material characteristics: a uniform and planar habit with well-controlled thickness, minimal defect/trapped charge density, a low resistance–area product for minimal power consumption, and compatibility with both the ferromagnetic metal and the semiconductor of choice, ensuring minimal diffusion to/from the surrounding materials at the temperatures required for device processing.

Metal Schottky barriers and oxide layers are susceptible to interdiffusion, interface defects and trapped charge, which have been shown to compromise spin injection/transport/detection. Ferromagnetic metals readily form silicides even at room temperature[19], and diffusion of the ferromagnetic species into the silicon creates magnetic scattering sites, limiting spin diffusion lengths and spin lifetimes in the silicon. Even a well developed and widely utilized oxide such as $SiO_2$ is known to have defects and trapped or mobile charge, which limit both charge and spin-based performance. Such approaches also result in contacts with high resistance–area products, and previous work has shown that smaller resistance–area products within a window of values are essential for efficient spin injection/detection[11,20], in addition to the more obvious benefit of reduced power consumption.

## Graphene as a tunnel barrier

Graphene, an atomically thin honeycomb lattice of carbon, offers a compelling alternative. Although it is very conductive in plane[21,22], it exhibits poor conductivity perpendicular to the plane[23]. Its $sp^2$ bonding results in a highly uniform, defect-free layer that is chemically inert, thermally robust, and essentially impervious to diffusion[24]. We have recently demonstrated that single-layer graphene can be used as a tunnel barrier between two metals in a magnetic tunnel junction, albeit with modest tunnel magnetoresistance[25]. Here, we show that a ferromagnetic metal/monolayer graphene contact serves as a spin-polarized tunnel barrier contact that successfully circumvents the classic metal/semiconductor conductivity mismatch issue for electrical spin injection into a semiconductor, and enables one to achieve contact resistance–area products that fall within the critical window of values required for practical devices[11,20]. We demonstrate electrical injection and detection of spin accumulation in silicon above room temperature, and show that the corresponding spin lifetimes correlate with the silicon donor concentration, confirming that the spin accumulation measured occurs in the silicon and not in the graphene or interface trap states. The resistance–area products are three orders of magnitude lower than those achieved with oxide tunnel barrier contacts on silicon substrates with identical doping levels. These results enable the realization of semiconductor spintronic devices such as spin-based transistors, logic and memory that rely on local magnetoresistance[4–7].

Graphene was grown by low-pressure chemical vapour deposition (CVD) within copper foil 'enclosures' according to ref. 26, and transferred onto hydrogen-passivated n-type silicon (001) substrates (electron density $n = 6 \times 10^{19}$ and $1 \times 10^{19}$ $cm^{-3}$). Raman spectroscopy confirmed that the graphene was of high quality with minimal defects[27]. During device fabrication, care was taken to

Naval Research Laboratory, Washington DC 20375, USA, †NRL Karle Fellows. *e-mail: vanterve@anvil.nrl.navy.mil; jonker@nrl.navy.mil

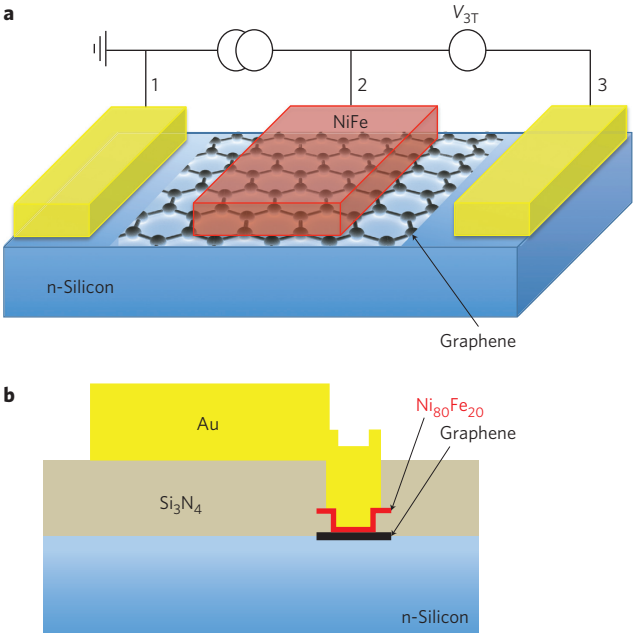


**Figure 1 | Schematic and cross-section of the samples. a**, Monolayer graphene serves as a tunnel barrier between the ferromagnetic metal contact and the Si substrate. Contacts 1 and 3 are ohmic Ti/Au contacts. **b**, The contact is designed so that the edges of the graphene are embedded in the SiN insulator, preventing conduction through the graphene edge states, which would short out the tunnel barrier.

isolate the conducting edges[28] of the graphene by burying them in a layer of sputter-deposited $Si_3N_4$ (Fig. 1). $Ni_{80}Fe_{20}$ was then sputter-deposited onto the graphene through vias in the $Si_3N_4$, defining the spin-polarized contacts, followed by another layer of $Si_3N_4$, and then electron-beam evaporation of ohmic Ti/Au contacts and bond pads. A schematic of the devices is provided in Fig. 1a,b. Electrical measurements were performed in a cryogen-free cryostat and electromagnet set-up using a three-terminal configuration, as depicted in Fig. 1a and described in the following. Further details may be found in the Supplementary Information.

Figure 2a shows the temperature dependence of the zero bias resistance (ZBR) for NiFe/monolayer graphene/Si ($6 \times 10^{19}$ cm$^{-3}$) contacts. The weak temperature dependence confirms that transport occurs by tunnelling through a pin-hole-free tunnel barrier, and provides a more definitive test for tunnelling than fits to a parabolic model[29]. The inset shows a typical nonlinear $I$–$V$ curve at 300 K.

Graphene serves as a highly conductive tunnel barrier, as demonstrated in Fig. 2b by a comparison of the room-temperature resistance–area products and current density versus voltage curves for three types of contact to the silicon ($6 \times 10^{19}$ cm$^{-3}$) substrate: NiFe/Si (ohmic), NiFe/graphene/Si (tunnelling) and NiFe/2 nm $SiO_2$/Si (tunnelling)[18] contacts. NiFe deposited directly on the silicon forms an ohmic contact with a resistance–area product of 0.4 kΩ μm$^2$, and the conductivity increases with decreasing temperature (metallic-like, Fig. 2a). When a single layer of graphene is inserted between the NiFe and the silicon, tunnelling behaviour dominates, but the resistance–area product increases to only 6 kΩ μm$^2$. In contrast, a NiFe/2 nm $SiO_2$ tunnel contact on the same substrate[18] has a much larger resistance–area product of 15 MΩ μm$^2$, with a corresponding decrease in the tunnel current of over a factor of $10^3$ at a given bias voltage. A similar trend is observed for contacts to the Si($1 \times 10^{19}$ cm$^{-3}$) substrate, although the NiFe/Si contact is Schottky-like rather than ohmic. Thus, the uniform atomically thin character of graphene provides a superior tunnel barrier with a low resistance–area product.

## A graphene solution to conductivity mismatch: spin injection

The large difference in conductivity precludes spin injection from a typical ferromagnetic metal into a semiconductor—the higher resistivity of the semiconductor limits current flow, so that equal amounts of majority and minority spin current flow into the semiconductor, resulting in zero net spin polarization[9–11]. A ferromagnetic metal/tunnel barrier provides a spin-selective interface resistance and circumvents this issue; the source term is the interface spin-polarized density of states of the ferromagnetic metal, and the higher tunnel barrier resistance controls the current flow[30].

Spin accumulation and precession directly under the magnetic tunnel barrier contact interface can be observed using a single contact for both spin injection and detection, as shown in Fig. 1a. A current is applied to contacts 1 and 2, and a voltage is measured

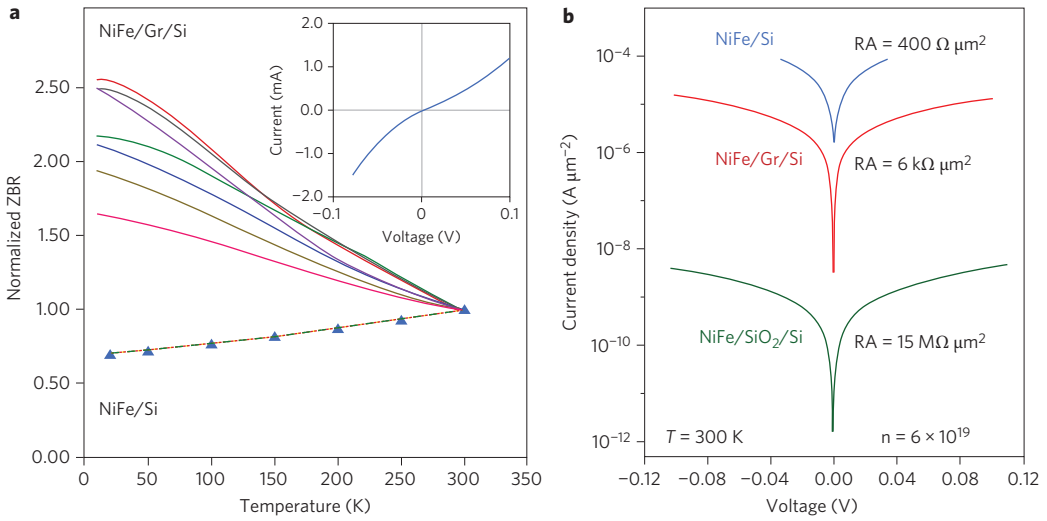


**Figure 2 | Electrical characteristics of the NiFe/graphene/Si contacts. a**, The normalized zero bias resistance (ZBR) shows a weak insulator-like temperature dependence, confirming tunnel transport. Each solid colour line is from a different contact, illustrating the reproducibility of the data. Inset: $I$–$V$ curve at 300 K. The ohmic NiFe/Si contacts exhibit metallic behaviour; results for three contacts are shown by triangles, red-dashed and green-dashed lines. **b**, Current–voltage curves and corresponding resistance–area (RA) products for NiFe/Si, NiFe/graphene/Si and NiFe/2 nm $SiO_2$/Si contacts. The Si electron density is $6 \times 10^{19}$ cm$^{-3}$.

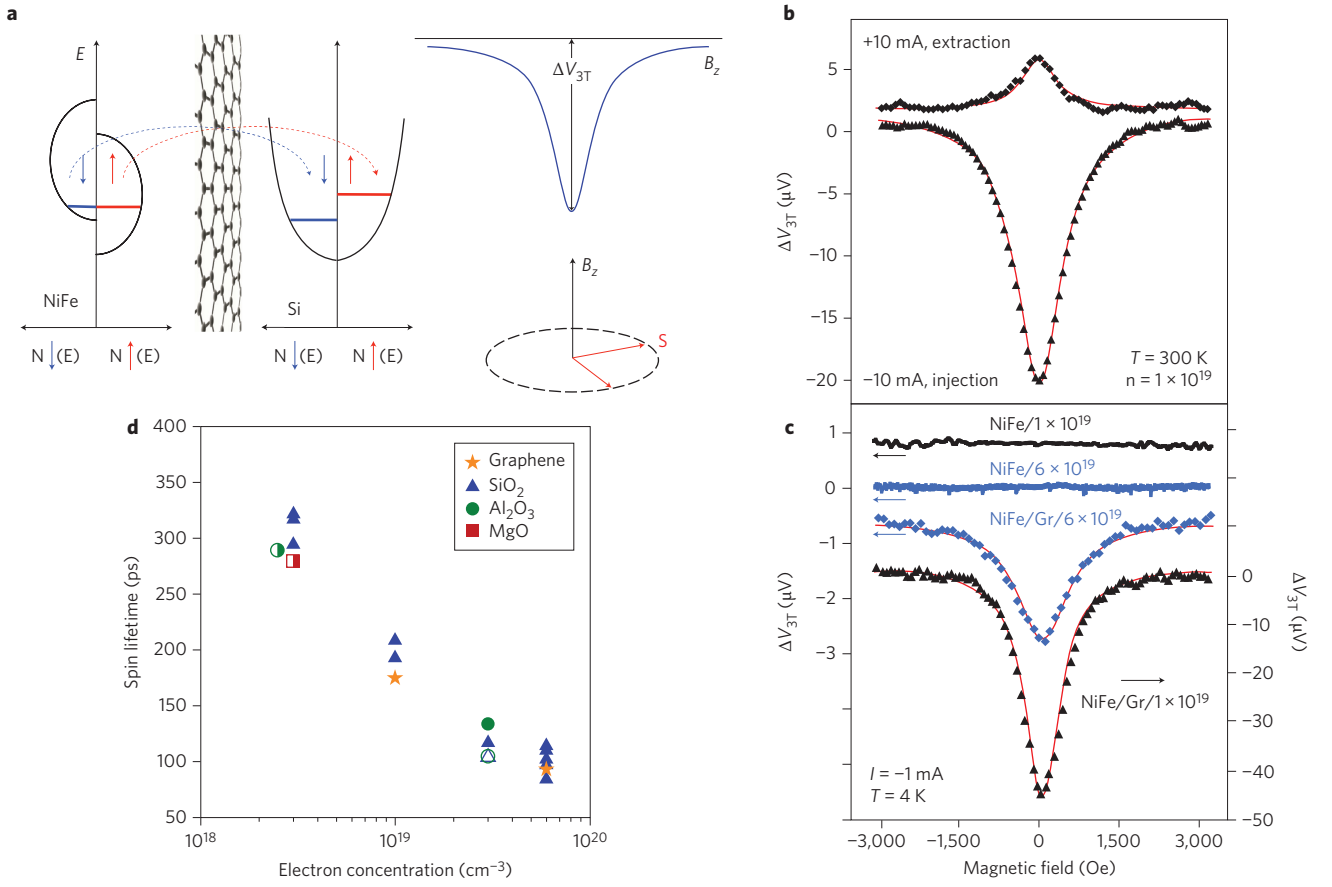


**Figure 3 | Hanle spin precession measurements. a**, Schematics illustrating spin injection, spin precession in an applied magnetic field, and the Lorentzian lineshape expected for an electrical measurement of the Hanle effect. N(E) refers to the energy-dependent density of states for majority spin (up arrow) and minority spin (down arrow) electrons. **b**, Room-temperature Hanle data for spin injection and extraction for the NiFe/graphene/Si ($1 \times 10^{19}$) samples using $40 \times 40$ μm$^2$ contacts. **c**, Low-temperature (4 K) Hanle data for the NiFe/Si ohmic reference contacts, and the NiFe/graphene/Si samples for both carrier concentrations studied. The red lines are fits to the experimental data using the Lorentzian function described in the text. The plots are offset for clarity, and every fifth data point is shown. **d**, Spin lifetimes obtained from three-terminal Hanle measurements at 10 K as a function of the Si electron density for the tunnel barrier materials indicated and different ferromagnetic metal contacts (Fe, CoFe, NiFe). Symbol shapes distinguish the tunnel barrier materials: triangles, $SiO_2$; circles, $Al_2O_3$; squares, MgO; stars, graphene. Solid symbols correspond to devices with $Ni_{0.8}Fe_{0.2}$ contacts, half-solid symbols to Fe contacts, and open symbols to $Co_{0.9}Fe_{0.1}$ contacts. The spin lifetimes show a pronounced dependence on the Si doping level, and little dependence on the choice of tunnel barrier or magnetic metal.

across contacts 2 and 3. The injection of spin-polarized carriers from ferromagnetic contact 2 produces a net spin accumulation in the silicon described by the splitting of the spin-dependent electrochemical potential, $\Delta\mu = \mu_{up} - \mu_{down}$ (Fig. 3a), which is detected as a voltage $\Delta V_{3T} = \gamma\Delta\mu/2e$, where $\gamma$ is the tunnelling spin polarization of the magnetic tunnel contact. When a magnetic field $B_z$ is applied perpendicular to the electron spin direction (sample surface), spin precession at the Larmor frequency $\omega_L = g\mu_B B_z/\hbar$ results in a reduction of the net spin accumulation due to precessional dephasing (the Hanle effect)[31]. Here, $g$ is the Lande $g$-factor ($g = 2$ for silicon), $\mu_B$ the Bohr magneton, and $\hbar$ the reduced Planck's constant. The voltage $\Delta V_{3T}(B_z)$ decreases with $B_z$ with a Lorentzian lineshape given by $\Delta V_{3T}(B_z) = \Delta V_{3T}(0)/[1 + (\omega_L\tau_s)^2]$ (ref. 31). Fits to this lineshape give a lower bound for the spin lifetime, $\tau_s$ (ref. 17).

Figure 3 presents data obtained from Hanle measurements of the NiFe/graphene/Si devices at room temperature (Fig. 3b) for spin injection and extraction, and at a low temperature (Fig. 3c) for spin injection for different silicon carrier concentrations, and for control samples. Devices incorporating a graphene tunnel barrier show a clear Hanle signal, confirming successful spin accumulation and field-induced precession. In contrast, control devices without graphene (Fig. 3c) show no signal, indicating that no significant spin accumulation occurs, as expected due to the large conductivity mismatch in the absence of a tunnel barrier.

Typical Hanle data are shown in Fig. 3b for a NiFe/graphene/Si ($1 \times 10^{19}$) sample at room temperature. When the contact is biased to inject electrons from the NiFe into the silicon, majority spin polarization builds in the silicon and a negative peak is observed in the Hanle signal at zero field. The magnitude of the spin voltage decreases with applied field $B_z$ as the spins precess and dephase, as described above. In the extraction case, a positive bias is applied to the NiFe, and majority spin electrons preferentially tunnel from the silicon into the NiFe, so that a minority spin polarization builds up in the silicon. In this case, the Hanle curve should reverse sign, and this behaviour is observed experimentally. Note that there is a significant difference between the magnitude of the Hanle signal in injection and extraction for a given bias current, as expected for an asymmetric metal/insulator/semiconductor structure (M/I/S). This also rules out spurious effects such as anisotropic magnetoresistance, which would exhibit equal amplitude upon reversing the bias. The measured spin voltage $\Delta V_{3T}(B_z = 0)$ is significantly larger at lower temperatures for a given bias current (Fig. 3c).

Values for the spin lifetime, $\tau_s$, are obtained from fits to the Hanle curves using the Lorentzian described above. Typical fits are shown by

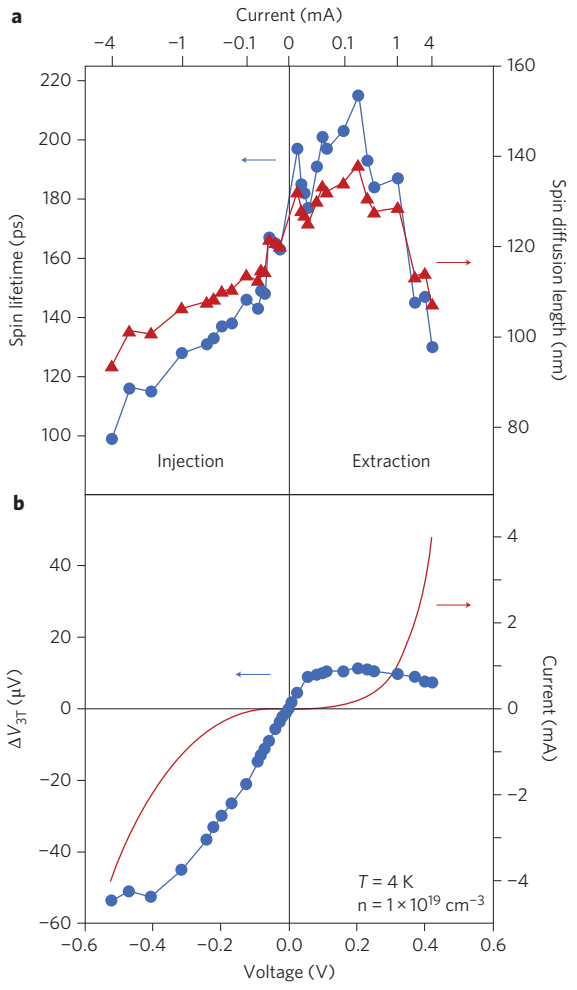


**Figure 4 | Bias dependence of spin lifetime/diffusion length and spin-voltage at 4 K. a**, Spin lifetime $\tau_s$ and diffusion length $L_{SD} = (D\tau_s)^{1/2}$ are at a maximum at low bias, and decrease with increasing positive and negative bias. **b**, Measured three-terminal spin voltage is strongly asymmetric with bias, although the conventional current–voltage characteristic is predominantly symmetric. The Si carrier concentration is $n = 1 \times 10^{19}$ cm$^{-3}$.

the solid lines in Fig. 3b,c, and yield values of $130 \pm 10$ ps at 300 K and a bias current of $\pm 10$ mA for the Si($1 \times 10^{19}$) sample. The spin lifetime depends strongly on contact bias and silicon donor density, and weakly on temperature due to the metallic character of the silicon, as discussed previously[18,32]. The spin lifetime decreases with increasing donor density, as expected from electron spin resonance (ESR) measurements on bulk silicon[32–34]. At $T = 4$ K, fits to the Hanle data of Fig. 3c yield $\tau_s = 140$ ps and 105 ps for the Si($1 \times 10^{19}$) and Si($6 \times 10^{19}$) samples, respectively.

These values agree well with those reported for NiFe/$SiO_2$ tunnel barrier contacts[18], and show a clear correlation with the character of the silicon. This is shown explicitly in Fig. 3d, where we plot the spin lifetime obtained from three-terminal Hanle data on n-Si as a function of electron density for four different tunnel barrier materials (graphene, $Al_2O_3$, MgO and $SiO_2$) and three different magnetic metal contacts (Fe, CoFe and NiFe). The spin lifetime measured with the three-terminal Hanle geometry shows a clear dependence only on electron density, and the dependence is consistent with literature ESR data on bulk silicon. The spin lifetime is completely independent of the tunnel barrier material or magnetic metal used for the contact. The values for the graphene tunnel barriers fall directly on the curve. These data confirm that the spin accumulation occurs in the silicon, and not in the graphene or possible interface trap states. The measured spin lifetimes are shorter than those in bulk silicon because they reflect the environment directly beneath the contact, where the reduced symmetry and increased scattering from the interface are likely to produce additional spin scattering[18].

## Bias and temperature dependence

The bias dependence of $\tau_s$ is summarized in Fig. 4a at $T = 4$ K for the Si($1 \times 10^{19}$) sample. At low bias, the spin lifetime is ~200 ps, and decreases to 100 ps with increasing negative bias (spin injection). For positive bias (spin extraction), $\tau_s$ initially increases slightly to 220 ps, and then decreases. The bias dependence is not fully understood, and a detailed discussion is beyond the scope of this text, but some qualitative observations can be made. The bias voltage alters the interface electric field and the electron energy, and hence the relevant portion of band structure involved. For spin injection, a negative bias is applied to the ferromagnetic/graphene tunnel contact, and both the interface electric field and the injected electron energy are increased. Both effects have been shown to reduce the measured spin lifetime. Hot electrons injected at higher energies into the host band structure experience rapid thermalization accompanied by spin relaxation[35], consistent with the trend we observe here. For spin extraction, the positive bias initially reduces the electric field, which exists due to carrier depletion at the silicon interface, and the modest increase in spin lifetime observed is consistent with this behaviour. Higher positive biases produce an interface electric field of opposite sign, pulling the electrons in the silicon towards the interface where the reduced symmetry and higher defect density are likely to produce more rapid spin relaxation, as observed experimentally. The electrons extracted from the silicon also sample the unfilled density of states of the NiFe where the polarization is lower[35]. This latter mechanism may change the spin extraction efficiency and hence the measured spin voltage (discussed below), but to first order should not strongly impact the spin lifetime measured in the silicon.

The measured spin voltage $\Delta V_{3T}(B_z = 0)$ produced by spin accumulation in the silicon also exhibits a strong bias dependence, as summarized in Fig. 4b together with the $I$–$V$ plot of the NiFe/graphene/Si($1 \times 10^{19}$) contact. Although the $I$–$V$ curve is approximately symmetrical, the $\Delta V_{3T}$–$V$ curve is markedly asymmetric, with much higher values achieved for spin injection than for extraction, as already noted in the Hanle data of Fig. 3b. For spin injection, $\Delta V_{3T}$ increases with the bias current as one might reasonably expect, despite the fact that the spin lifetime is decreasing, indicating that the spin source process more strongly affects the spin accumulation than the spin relaxation process. However, for spin extraction, $\Delta V_{3T}$ quickly saturates, even though the current is exponentially increasing with bias voltage. This may be attributed in part to a decrease in the spin lifetime (Fig. 4a), or to the bias dependence of the detection efficiency[36], or to less efficient spin filtering due to reduced spin polarization of the NiFe density of states above the Fermi level[35]. Further work is necessary to quantify the roles played by these various processes. Similar data were obtained for the Si($6 \times 10^{19}$) sample over $\pm 0.2$ V bias (limited by the maximum current allowed), and exhibited symmetric behaviour.

The spin diffusion length is given by $L_{SD} = (D\tau_s)^{1/2}$, where $D$ is the diffusion constant calculated from the measured carrier concentration and mobility using the Fermi–Dirac expansion for degenerate systems, $D = (2\mu kT/q)(F_{1/2}(\eta_F)/F_{-1/2}(\eta_F))$, where $F_{1/2}(\eta_F)$ and $F_{-1/2}(\eta_F)$ are the Fermi–Dirac integrals of order $1/2$ and $-1/2$, respectively, and $\eta_F = (E_F - E_C)/kT$ (ref. 37). Values at 4 K are shown in Fig. 4a as a function of bias for the Si($1 \times 10^{19}$) sample, and for both samples as a function of temperature in Fig. 5a. The temperature dependence mirrors that of the diffusion constant. $L_{SD}$ reaches a value ~200 nm near room temperature

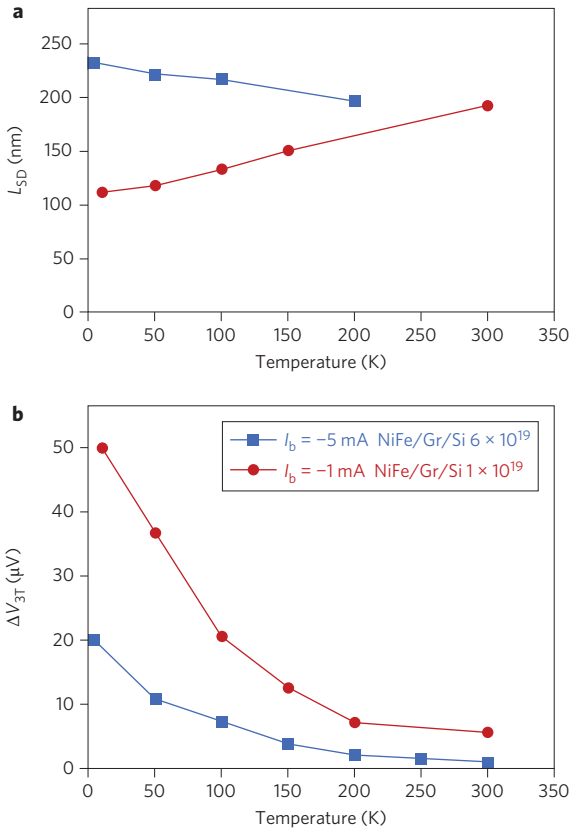


**Figure 5 | Temperature dependence of spin diffusion length and voltage.** **a**, Temperature dependence of $L_{SD}$ is dominated by that of the diffusion constant. **b**, Measured three-terminal spin voltage decreases monotonically with increasing temperature.

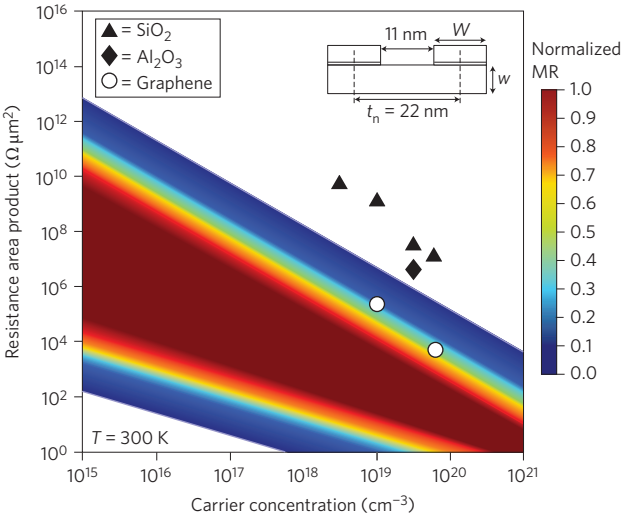


**Figure 6 | Resistance–area product window for local magnetoresistance.** Calculation of the local (two-terminal) magnetoresistance (MR) as a function of the conventional resistance–area product of the contact and the Si electron density for the device geometry shown in the inset, using the theory of ref. 11. Data points are the resistance–area products measured for our ferromagnetic metal/tunnel barrier/Si contacts using 2 nm $SiO_2$ (triangles), 1.5 nm $Al_2O_3$ (diamond) and monolayer graphene (circles) tunnel barriers prepared from identical Si wafers in our laboratory. The ferromagnetic metal/graphene resistance–area products fall within the window of useful magnetoresistance values. $W = w = 11$ nm.

for these carrier concentrations, demonstrating that practical devices based on spin transport in silicon are viable with conventional lithographic and fabrication techniques.

The measured spin voltage $\Delta V_{3T}(B_z = 0)$ decreases monotonically with temperature, as shown in Fig. 5b. The spin resistance–area product, defined as $\Delta V_{3T}(0)A/I_b$, where $A$ is the contact area and $I_b$ the bias current, is a useful metric for evaluating contact performance and for comparing experimental results with theory. For the higher biases used (producing larger spin voltages), the Si($1 \times 10^{19}$) and Si($6 \times 10^{19}$) samples exhibit spin resistance–area products of 72 Ω μm$^2$ and 0.84 Ω μm$^2$ respectively at $T = 4$ K, and 9 Ω μm$^2$ and 0.04 Ω μm$^2$ at 300 K. The spin resistance–area product predicted by the theory of diffusive transport across a single ferromagnetic metal/semiconductor interface for the geometry used here is given by $\gamma^2 r_1 = \gamma^2(\rho L_{SD})$ (refs 11,20), where $\rho$ is the sample resistivity and $L_{SD}$ is the spin diffusion length determined from the Hanle data as described above. If we assume a typical value for the tunnelling spin polarization $\gamma \approx 0.4$, the corresponding values for our samples are 1.2–1.8 Ω μm$^2$ ($1 \times 10^{19}$) and 0.2–0.3 Ω μm$^2$ ($6 \times 10^{19}$) over the temperature range 4–300 K. We thus see generally good agreement with the calculated results, although the bias dependence we observe experimentally has not been addressed theoretically.

## Resistance–area products

The conventional resistance–area product of the magnetic contact is an important parameter in determining the practical applications of spin-based semiconductor devices such as the silicon spin-MOSFET[5] (note that this is the standard resistance–area product rather than the spin resistance–area product discussed above). The operation of such devices depends on realizing significant local magnetoresistance, that is, the magnetoresistance measured directly between two magnetic contacts. Calculations have shown that significant local magnetoresistance can be achieved only if the contact resistance–area product falls within a range that depends on the silicon channel conductivity, the spin lifetime, the contact spacing (for example, the spin transistor gate length)[11,20] and the contact width[38]. The resistance–area products of all tunnel barrier contacts so far have been much larger than required, making such devices unattainable. However, the low resistance–area products provided by the graphene tunnel barriers fall within this window, and enable realization of these and other important spintronic devices. Previous work to lower the resistance–area product utilized a low-workfunction metal such as gadolinium at the tunnel barrier interface, but no spin accumulation in the semiconductor was demonstrated[39].

We calculated the range of optimum resistance–area products and the corresponding local magnetoresistance as a function of the silicon electron density based on the model of ref. 11, using the contact geometry shown as the inset to Fig. 6. The geometric parameters are chosen to be consistent with the node anticipated for silicon device technology within the next five years. The carrier concentration dependence of the mobility, resistivity and spin lifetime are taken from refs 32–34 and 37, and we assume that the Einstein relation between the mobility and diffusion constant holds for the complete doping range. The colour code in Fig. 6 identifies the range of useful magnetoresistance and the corresponding window of contact resistance–area products required.

Tunnel barrier contacts of ferromagnetic/$Al_2O_3$ and ferromagnetic/$SiO_2$ fabricated previously in our laboratory have been shown to produce significant spin accumulation in silicon[15,18], but have resistance–area products that are too high to generate usable local magnetoresistance. In contrast, utilizing monolayer graphene as the tunnel barrier lowers the resistance–area product by orders of magnitude, and values for the

NiFe/graphene contacts on bulk wafers fall well within the range required to generate high local magnetoresistance. Reducing the resistance–area product also has a positive effect on the electrical properties of the spin device, as lowering the resistance reduces noise and increases the speed of an electrical circuit[40].

## Conclusions

In summary, we have demonstrated that a ferromagnetic metal/monolayer graphene contact serves as a spin-polarized tunnel barrier contact, which successfully circumvents the classic metal/semiconductor conductivity mismatch issue for electrical spin injection and detection. Our results identify a route to low resistance–area product spin-polarized contacts, a crucial requirement enabling future semiconductor spintronic devices. Graphene provides a tunnel barrier with a uniform and planar habit, well-controlled thickness, minimal defect/trapped charge density, a low resistance–area product and compatibility with both the ferromagnetic metal and semiconductor of choice, ensuring minimal diffusion to/from the surrounding materials at the temperatures required for device processing. Utilizing multilayer graphene in such structures may provide much higher values of the tunnel spin polarization due to the band structure derived spin filtering effects that have been predicted for selected ferromagnetic metal/multilayer graphene structures[41–43]. Such an increase will improve the performance of semiconductor spintronic devices by providing higher signal-to-noise ratios and corresponding operating speeds, thereby advancing the technological applications of silicon spintronics[44].

Received 12 June 2012; accepted 17 August 2012; published online 30 September 2012

## References


1. *International Technology Roadmap for Semiconductors* (ITRS) (Semiconductor Industry Association, 2009); available at www.itrs.net
2. Awschalom, D. D. & Flatte, M. E. Challenges for semiconductor spintronics. *Nature Phys.* **3,** 153–159 (2007).
3. Zutic, I., Fabian, J. & Das Sarma, S. Spintronics: fundamentals and applications. *Rev. Mod. Phys.* **76,** 323–410 (2004).
4. Dery, H., Dalal, P., Cywinski, L. & Sham, L. J. Spin-based logic in semiconductors for reconfigurable large-scale circuits. *Nature* **447,** 573–576 (2007).
5. Sugahara, S. & Nitta, J. Spin-transistor electronics: an overview and outlook. *Proc. IEEE* **98,** 2124–2154 (2010).
6. Dery, H., Song, Y., Li, P. & Zutic, I. Silicon spin communication. *Appl. Phys. Lett.* **99,** 082502 (2011).
7. Tanaka, M. & Sugahara, S. MOS-based spin devices for reconfigurable logic. *IEEE Trans. Electron. Dev.* **54,** 961–976 (2007).
8. Behin-Aein, B., Datta, D., Salahuddin, S. & Datta, S. Proposal for an all-spin logic device with built-in memory. *Nature Nanotech.* **5,** 266–269 (2010).
9. Schmidt, G., Ferrand, D., Molenkamp, L. W., Filip, A. T. & van Wees, B. J. Fundamental obstacle for electrical spin injection from a ferromagnetic metal into a diffuse semiconductor. *Phys. Rev. B* **62,** R4790–R4793 (2000).
10. Rashba, E. I. Theory of electrical spin injection: tunnel contacts as a solution of the conductivity mismatch problem. *Phys. Rev. B* **62,** R16267–R16270 (2000).
11. Fert, A. & Jaffres, H. Conditions for efficient spin injection from a ferromagnetic metal into a semiconductor. *Phys. Rev. B* **64,** 184420 (2001).
12. Hanbicki, A. T. *et al.* Efficient electrical spin injection from a magnetic metal/tunnel barrier contact into a semiconductor. *Appl. Phys. Lett.* **80,** 1240–1242 (2002).
13. Hanbicki, A. T. *et al.* Analysis of the transport process providing spin injection through an Fe/AlGaAs Schottky barrier. *Appl. Phys. Lett.* **82,** 4092–4094 (2003).
14. Motsnyi, V. F. *et al.* Electrical spin injection in a ferromagnet/tunnel barrier/semiconductor heterostructure. *Appl. Phys. Lett.* **81,** 265–267 (2002).
15. Jonker, B. T., Kioseoglou, G., Hanbicki, A. T., Li, C. H. & Thompson, P. E. Electrical spin-injection into silicon from a ferromagnetic metal/tunnel barrier contact. *Nature Phys.* **3,** 542–546 (2007).
16. Sasaki, T. *et al.* Electrical spin injection into silicon using MgO tunnel barrier. *Appl. Phys. Exp.* **2,** 052003 (2009).
17. Dash, S. P., Sharma, S., Patel, R. S., de Jong, M. P. & Jansen, R. Electrical creation of spin polarization in silicon at room temperature. *Nature* **462,** 491–494 (2009).
18. Li, C. H., van't Erve, O. M. J. & Jonker, B. T. Electrical injection and detection of spin accumulation in silicon at 500 K with magnetic metal/silicon dioxide contacts. *Nature Commun.* **2,** 245 (2011).
19. Klasges, R. *et al.* Formation of a ferromagnetic silicide at the Fe/Si(100) interface. *Phys. Rev. B* **56,** 10801–10804 (1997).
20. Fert, A., George, J-M., Jaffres, H. & Mattana, R. Semiconductors between spin-polarized sources and drains. *IEEE Trans. Electron. Dev.* **54,** 921–932 (2007).
21. Novoselov, K. S. *et al.* Electric field effect in atomically thin carbon films. *Science* **306,** 666–669 (2004).
22. Zhang, Y., Tan, Y-W., Stormer, H. L. & Kim, P. Experimental observations of the quantum Hall effect and Berry's phase in graphene. *Nature* **438,** 201–204 (2005).
23. Krishnan, K. S. & Ganguli, N. Large anisotropy of the electrical conductivity of graphite. *Nature* **144,** 667–670 (1939).
24. Chen, S. *et al.* Oxidation resistance of graphene-coated Cu and Cu/Ni alloy. *ACS Nano* **5,** 1321–1327 (2011).
25. Cobas, E., Friedman, A. L., van't Erve, O. M. J., Robinson, J. T. & Jonker, B. T. Graphene as a tunnel barrier: graphene-based magnetic tunnel junctions. *Nano Lett.* **12,** 3000–3004 (2012).
26. Li, X. *et al.* Large-area graphene single crystals grown by low-pressure chemical vapor deposition of methane on copper. *J. Am. Chem. Soc.* **133,** 2816–2819 (2011).
27. Buchowicz, G. *et al.* Correlation between structure and electrical transport in ion-irradiated graphene grown on Cu foils. *Appl. Phys. Lett.* **98,** 032102 (2011).
28. Chae, J. *et al.* Enhanced carrier transport along edges of graphene devices. *Nano Lett.* **12,** 1839–1844 (2012).
29. Jonsson-Akerman, B. J. *et al.* Reliability of normal-state current–voltage characteristics as an indicator of tunnel-junction barrier quality. *Appl. Phys. Lett.* **77,** 1870–1872 (2000).
30. Jonker, B. T. in *Handbook of Spin Transport and Magnetism in Electronic Systems* (eds Tsymbal, E. & Zutic, I.) Ch. 17, 329–369 (CRC, 2012).
31. D'yakonov, M. I. & Perel', V. I. in *Optical Orientation, Modern Problems in Condensed Matter Science* Vol. 8 (eds Meier, F. & Zakharchenya, B. P.) 39 (North-Holland, 1984).
32. Ochiai, Y. & Matsuura, E. ESR in heavily doped n-type silicon near a metal-nonmetal transition. *Phys. Status Solidi (a)* **38,** 243–252 (1976).
33. Pifer, J. H. Microwave conductivity and conduction-electron spin-resonance linewidth of heavily doped Si:P and Si:As. *Phys. Rev. B* **12,** 4391–4402 (1975).
34. Zarifis, V. & Castner, T. G. ESR linewidth behavior for barely metallic n-type silicon. *Phys. Rev. B* **36,** 6198–6201 (1987).
35. Valenzuela, S. O., Monsma, D. J., Marcus, C. M., Narayanamurti, V. & Tinkham, M. Spin polarized tunneling at finite bias. *Phys. Rev. Lett.* **94,** 196601 (2005).
36. Crooker, S. A. *et al.* Bias-controlled sensitivity of ferromagnet/semiconductor electrical spin detectors. *Phys. Rev. B* **80,** 041305(R) (2009).
37. Sze, S. M. *Physics of Semiconductor Devices* 29 (Wiley, 1981).
38. Dery, H., Cywinski, L. & Sham, L. J. Lateral diffusive spin transport in layered structures. *Phys. Rev. B* **73,** 041306(R) (2006).
39. Min, B-C., Motohashi, K., Lodder, C. & Jansen, R. Tunable spin-tunnel contacts to silicon using low-work-function ferromagnets. *Nature Mater.* **5,** 817–822 (2006).
40. Cywinski, L., Dery, H. & Sham, L. J. Electric readout of magnetization dynamics in a ferromagnet–semiconductor system. *Appl. Phys. Lett.* **89,** 042105 (2006).
41. Karpan, V. M. *et al.* Graphite and graphene as perfect spin filters. *Phys. Rev. Lett.* **99,** 176602 (2007).
42. Karpan, V. M. *et al.* Theoretical prediction of perfect spin filtering at interfaces between close-packed surfaces of Ni or Co and graphite or grapheme. *Phys. Rev. B* **78,** 195419 (2008).
43. Yazyev, O. V. & Pasquarello, A. Magnetoresistive junctions based on epitaxial graphene and hexagonal boron nitride. *Phys. Rev. B* **80,** 035408 (2009).
44. Jansen, R. Silicon spintronics. *Nature Mater.* **11,** 400–408 (2012).


## Acknowledgements

This work was supported by core programmes at NRL and the Office of Naval Research. E.C. and A.L.F. acknowledge support from the NRL Karles Fellow programme. The authors acknowledge use of facilities in the NRL Nanoscience Institute, and thank D. Zapotok and D. St. Amand for continual technical support.

## Author contributions

O.M.J.v.E. and B.T.J. conceived the experiment. O.M.J.v.E., A.L.F., E.C. and C.H.L. fabricated the samples. J.T.R. grew the CVD graphene and transferred layers to the device structures. O.M.J.v.E. and C.H.L. acquired and analysed the transport data. All authors contributed to the interpretation of the data. O.M.J.v.E. and B.T.J. wrote the paper.

## Additional information

Supplementary information is available in the online version of the paper. Reprints and permission information is available online at http://www.nature.com/reprints. Correspondence and requests for materials should be addressed to O.M.J.v.a.E. and B.T.J.

## Competing financial interests

The authors declare no competing financial interests.